CrossMark

Diurnal cycle of precipitation over the British Isles in a 0.44° WRF multiphysics regional climate ensemble over the period 1990–1995

P. A. Mooney[1,2] · F. J. Mulligan[3] · C. Broderick[2,4]

Abstract The diurnal cycle of precipitation is an important and fundamental cycle in Earth's climate system, yet many aspects of this cycle remain poorly understood. As a result climate models have struggled to accurately simulate the timing of the peak and the amplitude of the cycle. This has led to a large number of modelling studies on the diurnal cycle of precipitation which have focussed mainly on the influence of grid spacing and/or convective parameterizations. Results from these investigations have shown that, while grid spacing and convective parameterizations are important factors in the diurnal cycle, it cannot be fully explained by these factors and it must also be subject to other factors. In this study, we use the weather research and forecasting (WRF) model to investigate four of these other factors, namely the land surface model (LSM), microphysics, longwave radiation and planetary boundary layer in the case of the diurnal cycle of precipitation over the British Isles. We also compare their impact with the effect of two different convective schemes. We find that all simulations have two main problems: (1) there is a large bias (too much precipitation) in both summer and winter (+19 and +38 % respectively for the ensemble averages), and (2) WRF summer precipitation is dominated by a diurnal (24-h) component (~28 % of the mean precipitation) whereas the observations show a predominantly semidiurnal (12-h) component with a much smaller amplitude (~10 % of mean precipitation). The choice of LSM has a large influence on the simulated diurnal cycle in summer with the remaining physics schemes showing very little effect. The magnitude of the LSM effect in summer is as large as 35 % on average and up to 50 % at the peak of the cycle. While neither of the two LSMs examined here capture the harmonic content of the diurnal cycle of precipitation very well, we find that use of the RUC LSM results in better agreement with the observations compared with Noah.

1 Introduction

The diurnal cycle of precipitation is an important and fundamental cycle in Earth's climate system which affects surface temperature range (Dai et al. 1999b), surface radiation (solar and terrestrial) and surface hydrology (Dai et al. 1999b). It has been studied extensively using surface and satellite measurements (Wallace 1975; Dai and Wang 1999; Dai et al. 1999a; Dai 2001a, b; Yang and Slingo 2001; Svensson and Jakob 2002; Dai et al. 2007; Twardosz 2007; Kikuchi and Wang 2008; Yaqub et al. 2011).

These studies show that most ocean regions have a weak diurnal cycle with a midnight to early morning peak in both seasons and a mean-to-peak amplitude between 10 and 30 % of the daily mean precipitation amount. Continental regions typically have a diurnal cycle with a morning peak

✉ P. A. Mooney
pmooney@ucar.edu

1 MMM Division, National Center for Atmospheric Research, Boulder, CO, USA

2 Department of Geography, Maynooth University, Maynooth, Kildare, Ireland

3 Department of Experimental Physics, Maynooth University, Maynooth, Kildare, Ireland

4 Lancaster Environment Centre, Lancaster University, Lancaster LA1 4YQ, UK

🍨 Springer

in winter and an afternoon-evening peak in summer. Furthermore, the mean-to-peak amplitude of the diurnal cycle in winter is much weaker than in summer; the summer values can range between 30 and 100 % of the daily mean precipitation amount.

There are exceptions to these observations and the diurnal cycle of precipitation in the Midwestern United States is one of the most widely known and studied examples. In this region, the warm season maximum occurs in the early morning rather than late afternoon. Numerous studies of this deviation (Dai et al. 1999a; Carbone et al. 2002; Lee et al. 2008) suggest that it arises from the eastward propagation of mesoscale convective systems originating in the Rocky Mountains in conjunction with the low-level jet east of the Rockies. Other regional differences exist (Oki and Musiake 1994; Dai et al. 1999a; Dai 2001a; Walther et al. 2013; Evans and Westra 2012) and many of these have been attributed to local effects such as land–sea breezes and mountain–valley circulations (Dai and Deser 1999; Mapes et al. 2003; Evans and Westra 2012). Although many characteristics of the diurnal cycle of precipitation are well known, both global climate models (GCMs) and regional climate models (RCMs) struggle to simulate the diurnal cycle of precipitation.

All models simulate the cycle with some success but there are large discrepancies. For example, most models simulate a maximum that occurs too early, with an amplitude that is too large over land and too small over oceans (Dai and Trenberth 2004; Collier and Bowman 2004; Walther et al. 2013; Jeong et al. 2011; Diro et al. 2012). While the overall amount of simulated precipitation can be close to the observed values, the frequency of precipitation occurrence is often too high and the average intensity of each occurrence is too low. Many studies (e.g. Dai et al. 1999a; Brockhaus et al. 2008; Clarke et al. 2007; Diro et al. 2012) have attributed this to an overly sensitive precipitation trigger mechanism in the models. Another well known feature of all models is that the diurnal cycle of warm season precipitation is more difficult to simulate than the winter diurnal cycle. These modelling challenges demonstrate that the current understanding of detailed regional characteristics and physical mechanisms that underlie the diurnal cycle remains incomplete.

This has led to a large number of modelling studies on the diurnal cycle to improve the agreement with observations and thereby elucidate the mechanisms that underlie the diurnal cycle of precipitation. In recent years it has received increased attention because an accurate representation of the amplitude and phase of the diurnal cycle is widely considered a good test of many aspects of the physical parameterizations in climate models (Collier and Bowman 2004; Brockhaus et al. 2008).

Many modelling studies have focussed on the influence of convective parameterizations and/or grid spacing on the diurnal cycle. Reducing the grid spacing has been shown to improve the model's ability to simulate the diurnal cycle of precipitation (Lee et al. 2007; Rauscher et al. 2010; Walther et al. 2013; Kendon et al. 2012; Dirmeyer et al. 2012). This is often attributed to the enhanced representation of complex terrain and land surface processes (Kendon et al. 2012). Furthermore, reducing the grid spacing to 'convection resolving' values (i.e., <~5km) can also improve the simulation of precipitation through improved representation of small scale convective processes (Brockhaus et al. 2008; Clarke et al. 2007; Kendon et al. 2012). Although increasing the horizontal resolution has been shown to reduce the bias in the simulated diurnal cycle, some bias still remains.

Warm season precipitation, which is the most difficult to simulate (Bukovsy and Karoly 2011), is largely controlled by convective processes at small spatial scales. For this reason a large number of studies (e.g., Liang et al. 2004; Brockhaus et al. 2008; Dirmeyer et al. 2012) have focused on the influence of convective parameterisation on a model's ability to simulate the diurnal cycle. These studies indeed show that simulated precipitation is sensitive to cumulus schemes and the skill of a scheme can depend on different climate regimes (Liang et al. 2004). In the case of the British Isles, Katragkou et al. (2015) report that all simulations in a weather research and forecasting (WRF) multi-physics ensemble which included three different cumulus schemes exhibited a wet bias.

Fewer studies have focused on the remaining parameterization categories since they are widely considered to have less influence on the diurnal cycle of precipitation. Diro et al. (2012) used the Regional Climate Model version 4 (RegCM4) to investigate the sensitivity of their simulations over Central America to the land surface models (LSM), community land model (CLM) and biosphere–atmosphere transfer scheme (BATS). Their research showed that total precipitation was sensitive to the land surface schemes. Furthermore, both simulations reproduced the amplitude of the observed cycle reasonably well but a systematic bias in the phase was common to both schemes. A study by Gianotti et al. (2012) which used the Regional Climate Model version 3 (RegCM3) showed that different LSMs [the biosphere–atmosphere transfer system version 1e (BATS1e) and the integrated biosphere simulator (IBIS)] influenced the model's ability to simulate the diurnal cycle with IBIS better than BATS1e.

In this study, we use the WRF model (ARW version 3.1; Skamarock et al. 2008) to investigate the impact of LSM, longwave radiation, microphysics, planetary boundary layer (PBL), and cumulus schemes on the diurnal cycle of precipitation. We focus specifically on the British Isles which is classified by the Köppen–Geiger system (Peel et al. 2007) as a temperate/mesothermal climate with significant precipitation in all seasons. This region was chosen based on the

availability of quality, high resolution observations which are described in Sect. 2. The results of our WRF simulations are compared with these observations to assess WRF's ability to simulate the cycle and its response to different parameterizations. Section 2 outlines details of the model set up and the observations. In Sect. 3, we compare precipitation amounts, frequency and intensity over the British Isles from our WRF multiphysics ensemble to hourly station data. Section 4 examines the influence of WRF parameterisations on the modelled diurnal cycle. We complete our study by exploring possible explanations for the different responses to the parameterisations examined.

2 Data and analysis methods

Our study of the diurnal cycle of precipitation is based on dividing each day into 3-h periods along the lines adopted in previous studies (e.g. Dai et al. 1999a; Evans and Westra 2012). In this case an occurrence is defined as an amount >0.1 mm in a 3-h period. The total precipitation in a 3-h period divided by the number of occurrences gives the intensity per occurrence in that 3-h period. We focus exclusively on winter (DJF) and summer (JJA) precipitation because summer is a known challenge for RCMs and winter is its contrasting season.

Previous studies on precipitation in the British Isles (Alexander and Jones 2000; Jones et al. 2014) have identified different climatic regions with similar rainfall characteristics. In this study, the effect of different climatic regions on the diurnal cycle of precipitation was investigated using the clustering technique employed by Argüeso et al. (2011) and Perez et al. (2014). Four different regions were identified with cluster groupings as follows: 3 stations in the

North West of Great Britain, 8 stations in the North East, 14 stations on the West coast, and 43 stations in the East and South-East. The differences between the 3-hourly precipitation values of the clusters at all eight times were small compared with the uncertainties of those values. Proceeding with the four clusters in this circumstance would be meaningless, and the analysis of all 68 stations was undertaken without disaggregation.

Harmonic analysis (e.g., Wallace 1975; Dai et al. 1999a; Yang and Slingo 2001; Collier and Bowman 2004; Diro et al. 2012) was applied to the simulated and observed data to quantify the percentage of variance explained by the diurnal (24-h) and semidiurnal (12-h) components. The average of each set of eight 3-hourly samples was subtracted from the set, and the resulting series as a function of time, t, in hours was fit using least squares regression to the following function:

$$a_{24} \cos(2\pi(t - \phi_{24})/24) + a_{12} \cos(2\pi(t - \phi_{12})/12),$$

where $a_{24}(a_{12})$ and $\phi_{24}(\phi_{12})$ are the amplitude and phase respectively of the diurnal (semidiurnal) harmonics.

2.1 Modelled data

A complete description of the WRF multiphysics ensemble used in this study can be found in Mooney et al. (2013), and only a brief summary is included here for completeness. The ensemble consists of thirteen WRF simulations driven by ERA-Interim (Dee et al. 2011) over the period 1989–1995. The simulations cover the European domain shown in Fig. 1. This domain complies with the World Climate Research Programme (WCRP) coordinated regional climate downscaling experiment (CORDEX) region 4 (http://wcrp-cordex.ipsl.jussieu.fr/images/pdf/cordex_regions.pdf)
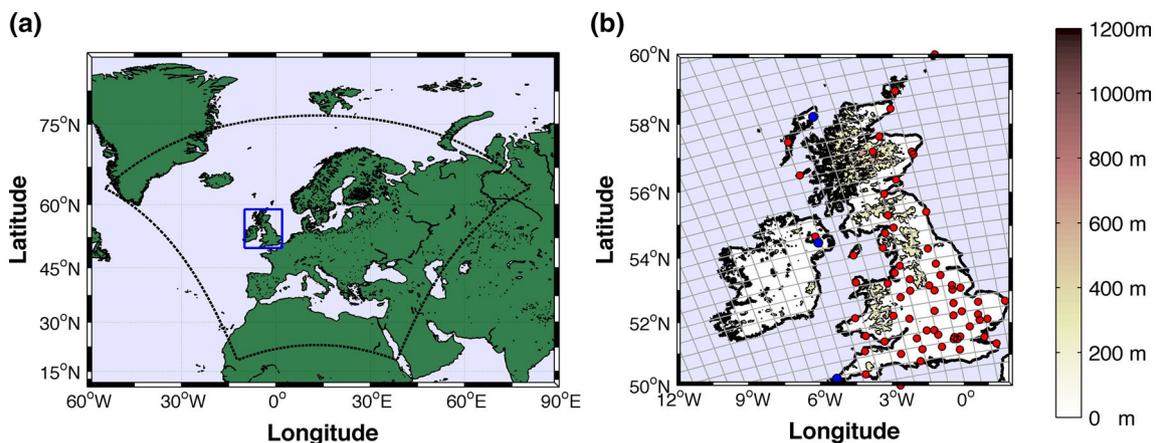
Fig. 1 a Map of Europe showing the (Euro-CORDEX) modelled domain (*dashed black lines*) and British Isles Rockel regions (Christensen and Christensen 2007) (*solid blue lines*). **b** Map of the British Isles Rockel region showing the WRF grid (*light grey lines*), the MIDAS stations (*red*) and UK Upper Air Network stations (*blue dots*) used in this study

Table 1 Physical parameterisations schemes used in each of the WRF simulations

Simulation name	Microphysics	PBL scheme	Land surface model	Longwave radiation	Cumulus scheme
W3_Ys_No_Rr	WSM3	YSU	Noah	RRTM	Kain–Fritsch
W3_Ys_No_Ca	WSM3	YSU	Noah	CAM	Kain–Fritsch
W3_Ys_Ru_Rr	WSM3	YSU	RUC	RRTM	Kain–Fritsch
W3_Ys_Ru_Ca	WSM3	YSU	RUC	CAM	Kain–Fritsch
Mo_Ys_No_Rr	Morrison	YSU	Noah	RRTM	Kain–Fritsch
Mo_Ys_No_Ca	Morrison	YSU	Noah	CAM	Kain–Fritsch
Mo_Ys_Ru_Rr	Morrison	YSU	RUC	RRTM	Kain–Fritsch
Mo_Ys_Ru_Ca	Morrison	YSU	RUC	CAM	Kain–Fritsch
Mo_My_No_Rr	Morrison	MYNN3	Noah	RRTM	Kain–Fritsch
Mo_My_No_Ca	Morrison	MYNN3	Noah	CAM	Kain–Fritsch
Mo_My_Ru_Rr	Morrison	MYNN3	RUC	RRTM	Kain–Fritsch
Mo_My_Ru_Ca	Morrison	MYNN3	RUC	CAM	Kain–Fritsch
W3_Ys_No_Rr_B	WSM3	YSU	Noah	RRTM	Betts–Miller–Janjic

W3 WRF single moment 3-class scheme (WSM3), *Mo* Morrison two-Moment scheme (Morrison), *Ys* Yonsei University (YSU), *My* Mellor–Yamada Nakanishi and Niino Level 3.0 (MYNN3), *No* Noah land surface model (NOAH), *Ru* rapid update cycle (RUC) LSM, *Rr* rapid radiative transfer model (RRTM), *Ca* community atmosphere model (CAM), *BMJ* Betts–Miller–Janjic

which uses a grid spacing of 0.44°. Previous studies on the effects of higher spatial resolution have reported no clear benefit unless the grid spacing is approximately 6 km or less (Walther et al. 2013; Jaeger et al. 2008). The computational cost of such a high resolution over a large domain for an extended period when several parameterizations are being investigated is difficult to justify. As discussed in Mooney et al. (2013), the model is allowed to spin up for 1 year and the period covering 1990–1995 is used in the analysis. Table 1 summarises the parameterizations used in each of the 13 simulations. All simulations use the community atmosphere model (CAM) shortwave radiation scheme (Collins et al. 2004). Two schemes have been included from each of the other five parameterization categories in WRF in an attempt to assess the level of sensitivity to each category. The two microphysics schemes employed are the Morrison two-moment scheme (Morrison et al. 2009) and WRF single moment 3-class scheme (WSM3; Hong et al. 2004). They are a good example of a computationally demanding complex scheme and a relatively simple scheme, respectively. Likewise, the two PBL schemes chosen—Yonsei University (YSU; Hong et al. 2006) and the Mellor–Yamada Nakanishi and Niino Level 3.0 (MYNN3) scheme (Mellor and Yamada 1982; Nakanishi and Niino 2004) are quite distinct from each other. Of the four LSMs available in this version of WRF, Noah (Ek and Mahrt 1991) and the rapid update cycle (RUC; Smirnova et al. 1997, 2000) are the only two that are suitable for regional climate modelling and are the most frequently used LSMs in WRF climate simulations (Bukovsy and Karoly 2009; Jin et al. 2010; Zeng et al. 2012; Evans and Westra 2012). The two longwave radiation schemes examined—rapid radiative transfer model (RRTM; Mlawer

et al. 1997) and community atmosphere model (CAM; Collins et al. 2004) are the two most suitable schemes available in WRF version 3.1 for regional climate simulations. We also examined the impact of two different cumulus parameterizations (CP) schemes—the Kain–Fritsch (CP) scheme (Kain and Fritsch 1990; Kain 2004) and the Betts–Miller–Janjic scheme (Betts 1986; Betts and Miller 1986; Janjic 1994). The results of these simulations are compared with the observational data described in the following section.

For comparison with the observations, simulation values are obtained by calculating the seasonal (winter or summer) 3-hourly average of the relevant parameter over every grid box that contains one of the observing stations shown in Fig. 1b. Comparing seasonal averages over tens of grid boxes with an average over an equal number of observing stations avoids the problem of the incomparability of precipitation at a single point with the amount averaged over an individual grid box which is also prone to 'noise' caused by synoptic and mesoscale variability that may blur the convective peak (Brockhaus et al. 2008).

2.2 Observational data

Hourly data used in this study was obtained from the UK Met Office Integrated Data Archive System (MIDAS; Met Office 2012) land and marine surface station data. This is a database of land and marine surface observations from the UK Met Office station network and a selection of other stations from around the world. Stations are archived with daily, hourly or sub-hourly observations depending on the availability of the measurements. In our study of the British Isles, we used only those stations that recorded hourly

data and covered more than 80 % of the time period. These criteria resulted in a total of 68, 38 and 36 eligible stations (shown in Fig. 1b) for precipitation, air temperature and relative humidity respectively. Whisker and boxplots for the observations were calculated based on 1000 bootstrapped samples and provide an estimation of the confidence intervals around the observed values.

Radiosonde data was obtained from the UK Upper Air Network (Met Office 2006) which is comprised of eight operational stations that record data up to four times per day. However, only three of these stations (Camborne, Hillsborough and Stornoway shown as blue dots in Fig. 1b) cover more than two-thirds of the time period investigated in this study.

3 Results

3.1 Observed seasonal mean diurnal cycle of the British Isles

Figure 2 shows the modelled and observed total amount of precipitation, occurrence and intensity for winter (left panels) and summer (right panels) averaged over the 68 stations shown in Fig. 1b. The corresponding ERA-Interim data (blue line) are also included in the plots. ERA-Interim values are offset in time with respect to the WRF values as they are available at different intervals to the WRF simulations. Precipitation in the British Isles is primarily frontal and orographic in origin, with convective precipitation evident only in summer (de Leeuw et al. 2014). Figure 2d–f show a primary peak in the total amount, occurrence and intensity of summer precipitation between 1400 and 1700 UTC. Also evident is a secondary peak between 0200 and 0500 UTC. Observations for western Europe reported by other studies (e.g., Kiely et al. 1998; Svensson and Jakob 2002; Walther et al. 2013) also show a diurnal and semi-diurnal cycle of summer rainfall with a primary peak in the mid-afternoon and a secondary peak near dawn.

Table 2 summarises the results of the harmonic analysis in which the phase of each harmonic indicates the time of maximum value of that component. The percentage values in the rows labeled 24-h amplitude (and 12-h amplitude) are the contribution of that component to the variance. In summer, total precipitation is a combination of a diurnal (24-h) component and a semidiurnal (12-h) harmonic which is almost twice as large. This contrasts with winter which consists primarily of a diurnal cycle with little evidence of a semi-diurnal component. The diurnal cycle of total amount of winter precipitation has a broad peak that occurs between 0800 and 1700 UTC. The broad shape of this peak, which will be discussed further in Sect. 4, is a result of the offset in the timings of the peak in precipitation occurrence and intensity.

### 3.2 Modelled seasonal mean diurnal cycle of the British Isles

Figure 2 also shows the modelled diurnal cycle of total amount of precipitation, occurrence and intensity per occurrence in winter and summer. These modelled results represent only those grid boxes which contain station data. It is clear from Fig. 2a–f, that WRF generally overpredicts the total precipitation and the number of occurrences but underpredicts the intensity of occurrence in both seasons. ERA Interim shows a similar trend. Furthermore, there is a much greater spread in the WRF simulations of the summer diurnal cycle compared to winter. In both seasons, WRF generally simulates the timing of the primary peak between 1400 and 1700 UTC correctly but it does not simulate the secondary peak in summer that is evident in the observed record between 0200 and 0500 UTC. WRF also overestimates the amplitude of the summer diurnal cycle by a factor of at least three on average.

Table 2 highlights the main differences between the observations and the ensemble average in winter and summer. It shows that WRF captures the observed diurnal cycle of total winter precipitation but poorly represents the warm season diurnal cycle. In summer, the modelled precipitation is dominated by the 24-h harmonic whereas the 12-h component is far more prevalent in the observations. Additionally, the simulated amount of precipitation and number of occurrences are too large by approximately 40 and 120 % respectively.

Overprediction of precipitation in regional climate models can arise from a wet bias in the driving data (Gianotti et al. 2012). However, this is an unlikely explanation as Fig. 2 shows that ERA-Interim does not have a large wet bias. Although, ERA-Interim does not capture the observed diurnal cycle well, the average total precipitation for ERA-Interim in summer (18.6 mm) and winter (28.2 mm) compares favourably with the observations in summer (18.7 mm) and winter (27.9 mm).

Figure 2b shows that all WRF simulations poorly reproduce the characteristics (amplitude and phase) of the diurnal cycle of precipitation occurrence in winter. The characteristics of the same cycle in summer (Fig. 2e) are also poorly simulated and WRF fails to capture the semi-diurnal cycle evident in the observed record. Furthermore, WRF models a peak time of 2000–2300 UTC in the occurrence of winter precipitation and a peak time of 1100–1400 UTC in summer. This is in contrast with the observations which show a peak between 0800–1100 UTC in winter and 0200–0500 UTC in summer.

Figure 2c shows that in winter WRF captures the diurnal cycle of precipitation intensity very well with a peak at 1400–1700 UTC which agrees with the observed record. Similarly, WRF simulates the amplitude of the 24-h winter intensity variation of 0.02 mm/h which agrees with the
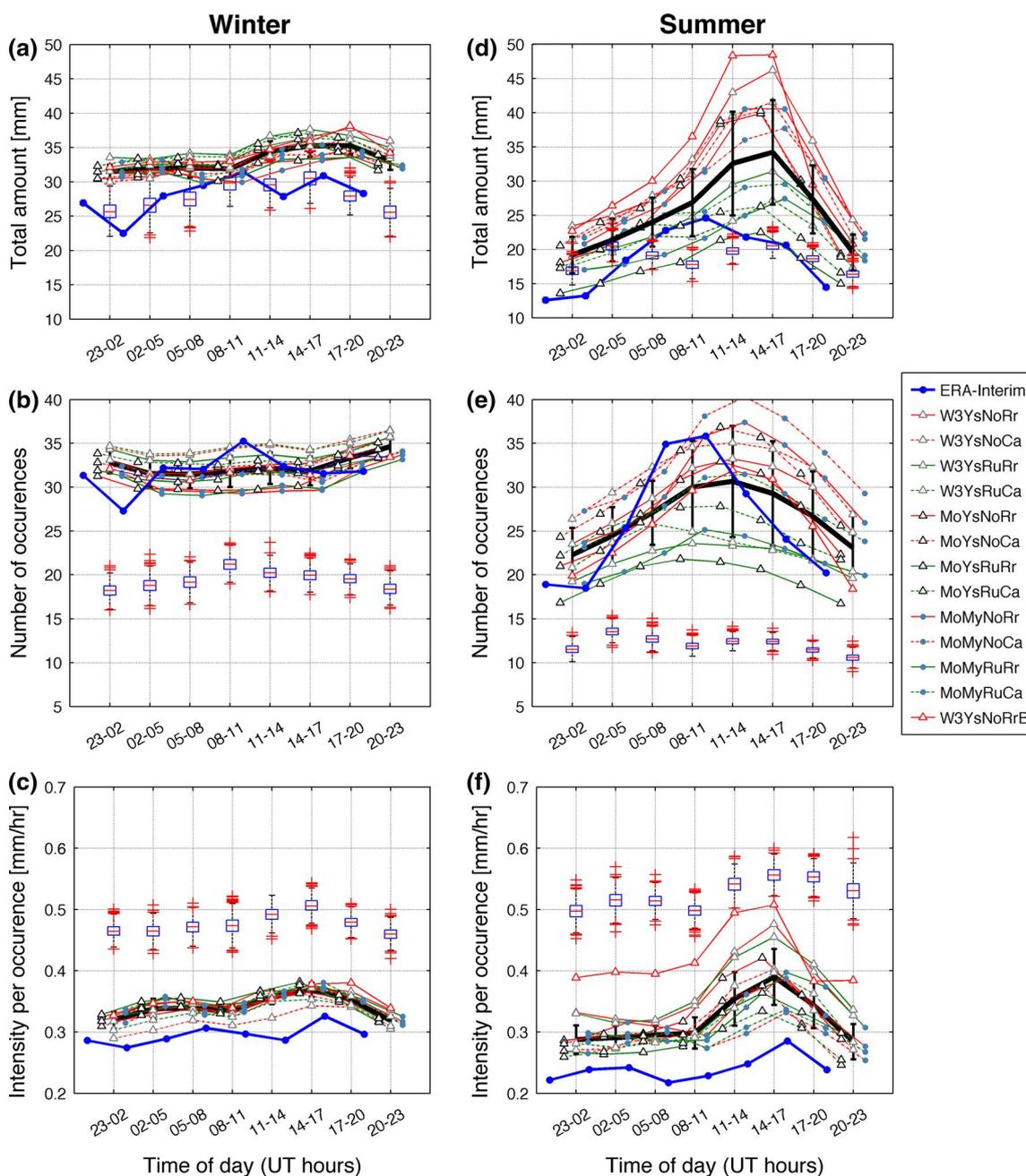
Fig. 2 a Diurnal cycle of total amount of precipitation (in mm during the 3 months of winter) averaged over 68 stations in the British Isles over the entire winter (DJF) period for observations (*boxplots*), 13 simulations listed in Table 1 (*red* and *green lines*), ensemble average (*black line*) and ERA-Interim (*blue line*). *Whisker* and *boxplots* for the observations were calculated based on 1000 bootstrapped samples for each 3-h time interval. *Error bars* on the ensemble average are the standard deviation of the 13 simulations for the 3-h interval. ERA-Interim values are offset with respect to the WRF values as they are available at different intervals to the WRF simulations. **b** As in **a** but showing the number of occurrences (threshold ≥0.1 mm) in each 3-h time interval over the entire winter period. **c** As in **a** but showing the intensity of precipitation per occurrence in each 3-h time interval. **d–f** As in **a–c** but for the summer (JJA) season

observed amplitude (see Table 2). Figure 2f shows that WRF captures the timing of the primary peaks of intensity in summer, but over-predicts the amplitude. Figure 2b, c show that WRF over-predicts the occurrence of winter precipitation and under-predicts the intensity during winter.

While these opposing biases tend to cancel each other to some extent, total precipitation amount is still overestimated by WRF.

Table 2 also includes results of harmonic analysis for ERA-Interim driving data. In winter, ERA Interim agrees

Table 2 Results of harmonic analysis of total precipitation, occurrence, and intensity for observed, ensemble average and ERA Interim (winter and summer)

	Winter						Summer					
	Observed	Var. (%)	Ensemble	Var. (%)	ERA Interim	Var. (%)	Observed	Var.	Ensemble	Var. (%)	ERA Interim	Var. (%)
Total precipitation (3-h values) (mm)												
Diurnal average (mm)	27.9 (1.9)		33.3 (1.6)		28.2 (2.8)		18.7 (1.6)		25.8 (5.8)		18.6 (4.6)	
24-h Amplitude (mm)	2.4 (0.3)	80	1.9 (0.2)	76	2.7 (0.8)	48	1.0 (0.3)	22	7.3 (0.2)	78	6.0 (0.4)	85
24-h Phase (h)	−11.4 (0.4)		−7.9 (0.2)		−9.8 (0.3)		11.2 (1.1)		−10.6 (0.05)		−11.6 (0.3)	
12-h Amplitude (mm)	0.4 (0.3)	2	0.6 (0.2)	8	1.9 (0.8)	23	1.8 (0.3)	61	2.5 (0.2)	9	0.7 (0.4)	1
12-h Phase (h)	−3.7 (1.7)		4.7 (0.8)		−3.1 (0.8)		3.8 (0.4)		3.3 (0.2)		−4.3 (0.2)	
Number of occurrences (3-h values)												
Diurnal average (mm)	19.4 (1.0)		32.4 (1.0)		31.7 (2.2)		12.1 (0.9)		26.9 (3.2)		25.9 (6.9)	
24-h Amplitude (mm)	1.2 (0.3)	73	1.0 (0.1)	55	2.0 (0.8)	44	0.8 (0.1)	38	4.2 (0.2)	87	8.8 (0.3)	82
24-h Phase (h)	11.9 (0.8)		−3.7 (0.5)		−10.7 (0.9)		7.8 (0.8)		−11.8 (0.1)		11.6 (0.1)	
12-h Amplitude (mm)	0.2 (0.3)	2	0.7 (0.1)	30	1.3 (0.8)	17	0.9 (0.1)	46	0.2 (0.2)	0	2.3 (0.3)	5
12-h Phase (h)	−3.1 (2.1)		−2.2 (0.3)		−1.9 (1.7)		3.6 (0.3)		4.7 (2.2)		−1.8 (0.3)	
Intensity per occurrence (mm/h)												
Diurnal average (mm/h)	0.48 (0.02)		0.34 (0.02)		0.3 (0.02)		0.53 (0.02)		0.32 (0.04)		0.3 (0.02)	
24-h Amplitude (mm/h)	0.02 (0.003)	67	0.019 (0.001)	53	0.12 (0.005)	28	0.03 (0.01)	62	0.046 (0.002)	70	0.016 (0.005)	30
24-h Phase (h)	−9.6 (0.12)		−10.3 (0.1)		−8.3 (0.5)		−7.3 (0.4)		−9.1 (0.01)		−5.9 (1.1)	
12-h Amplitude (mm/h)	0.01 (0.003)	16	0.015 (0.001)	34	0.01 (0.005)	36	0.01 (0.004)	18	0.023 (0.002)	17	0.021 (0.005)	49
12-h Phase (h)	3.5 (0.6)		4.1 (0.2)		−4.3 (0.1)		4.2 (0.9)		3.4 (0.2)		5.3 (0.5)	

The figures in parentheses are the $1 - \sigma$ uncertainties on the quoted values estimated from the least-squares fit. The percentage values in the rows labeled diurnal (and semidiurnal) amplitude are the contribution of that component to the variance

remarkably well with the observations for average total precipitation, while the WRF ensemble average is approximately 20 % too high. However, the distribution of the explained variance between the diurnal and semidiurnal components in WRF is much closer to the observations than ERA Interim. This trend is also evident in the number of occurrences and in the intensity per occurrence in winter.

In summer, ERA Interim also agrees with the observations for the average total precipitation, and the WRF ensemble is too high by nearly 40 % in this season. The distribution of the explained variance between the diurnal and semidiurnal components in both ERA Interim and the WRF ensemble is quite different to the observations in summer. Both WRF and ERA-Interim show very dominant diurnal components and negligible semidiurnal components, whereas the observations have a dominant semidiurnal component. However, WRF shows better agreement with the distribution of the harmonic content of total precipitation and intensity per occurrence compared with ERA Interim.

In this section we have described the general behaviour of the WRF model. There are substantial differences between the simulations which are explored in the following section.

4 Influence of WRF parameterizations on the modelled seasonal mean diurnal cycle of precipitation

Figure 3a–f show the influence of the LSM on the diurnal cycle of the total amount of precipitation, number of occurrences and intensity per occurrence in both winter (left panels) and summer (right panels). The ensemble averages of the WRF simulations which use Noah and those which use RUC are plotted as continuous lines with error bars representing the maximum and minimum bounds of the 6 simulations in each ensemble. This facilitates easy comparison of modelled and observed values (boxplots) of the diurnal cycle of (a) total precipitation, (b) the number of occurrences and (c) the intensity per occurrence in each 3-h period in both winter and summer. Figure 4a–f show the influence of the microphysics parameterizations on the diurnal cycle of precipitation using the format of Fig. 3a–f, while Figs. 5a–f, 6a–f and 7a–f show the influence of longwave radiation, PBL, and cumulus schemes respectively on the modelled diurnal cycle of precipitation.

4.1 Influence of land surface models

Figure 3a–c show that the LSM have a negligible impact in winter. This agrees with a study by Jin et al. (2010) which showed that winter precipitation over the western United States simulated by WRF was largely unaffected by four different LSMs. Jin et al. (2010) also showed that WRF consistently overestimated precipitation in agreement with our results in Sect. 3.

In contrast to winter, Fig. 3d–f show that LSMs clearly influence the model's ability to simulate the diurnal cycle of precipitation in summer. In summer, simulations using RUC clearly agree better with the observed diurnal cycle of total precipitation and number of occurrences than simulations using Noah. Figure 3d shows that simulations of average total precipitation during the night time (2000–0800 UTC) using the RUC LSM are in good agreement with observations but daytime values are almost 30 % in excess. This result agrees with Gianotti et al. (2012) who found that RegCM3 simulations of the Maritime Continent were sensitive to LSMs. On the other hand Diro et al. (2012) reported that, while certain aspects of precipitation over Central America were sensitive to the land surface schemes, when using the RegCM4 model they observed little impact on the diurnal cycle of precipitation in their simulations. The very different geographic region employed in the latter case may be the explanation of the different outcome in that instance.

The LSMs show no influence on the timing of the primary peak of the diurnal cycle of total amount and intensity but they do influence the peak timing in the number of occurrences. In this instance, Noah and RUC simulate different timings but neither of them capture it accurately.

4.2 Influence of microphysics schemes

Figure 4a–f show that the two microphysics schemes (WSM3 and Morrison), chosen because they represent widely differing complexity and computational cost, have a negligible influence on the diurnal cycle of precipitation in winter and a small influence on summertime precipitation. In summer, both schemes poorly reproduce the characteristics of the diurnal cycle of total amount but simulations using the Morrison scheme have a slightly smaller bias than those using WSM3. The large range in summer of the four simulations for each microphysics scheme (indicated by the error bar in Fig. 4d, e) results from the large difference between the LSMs (described in Sect. 4.1) in each group of four. Figure 4e shows that microphysics has a negligible impact on the diurnal cycle of precipitation occurrence in summer. However, Fig. 4f shows that the microphysics schemes marginally influence the model's ability to simulate the amplitude of the diurnal cycle of intensity. Simulations using the Morrison scheme have an amplitude closer to the observed cycle but it has a larger bias than those simulations using WSM3.
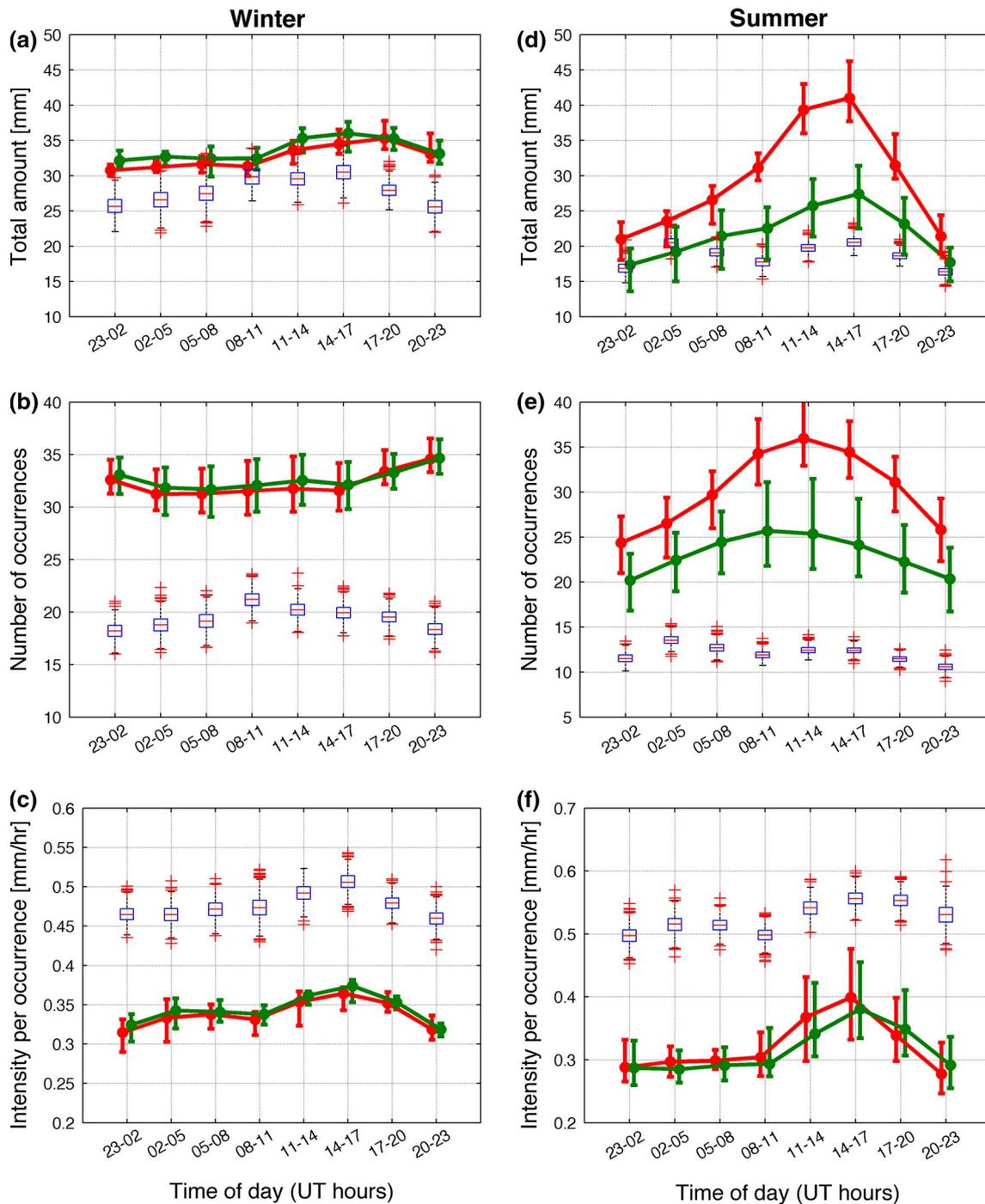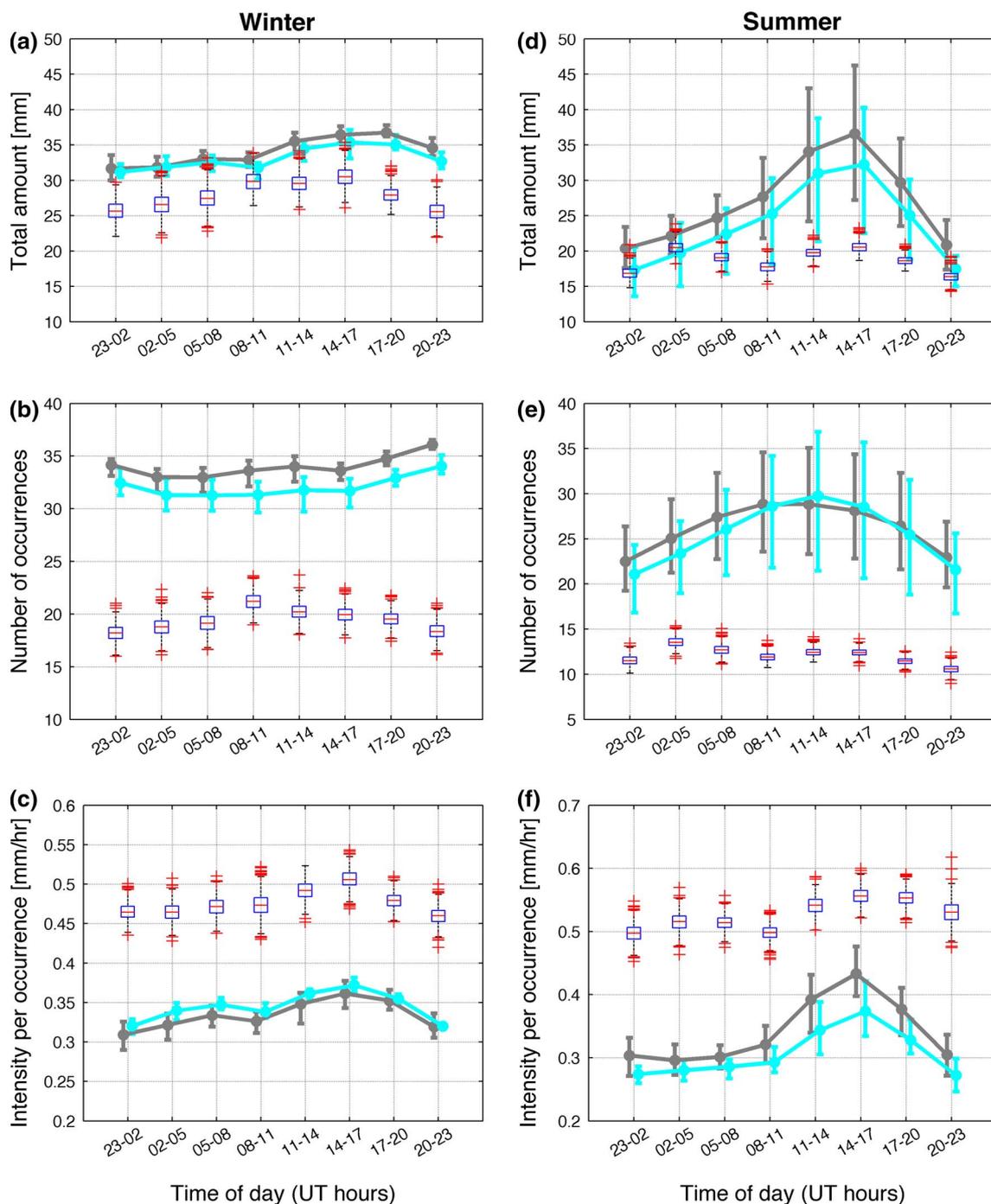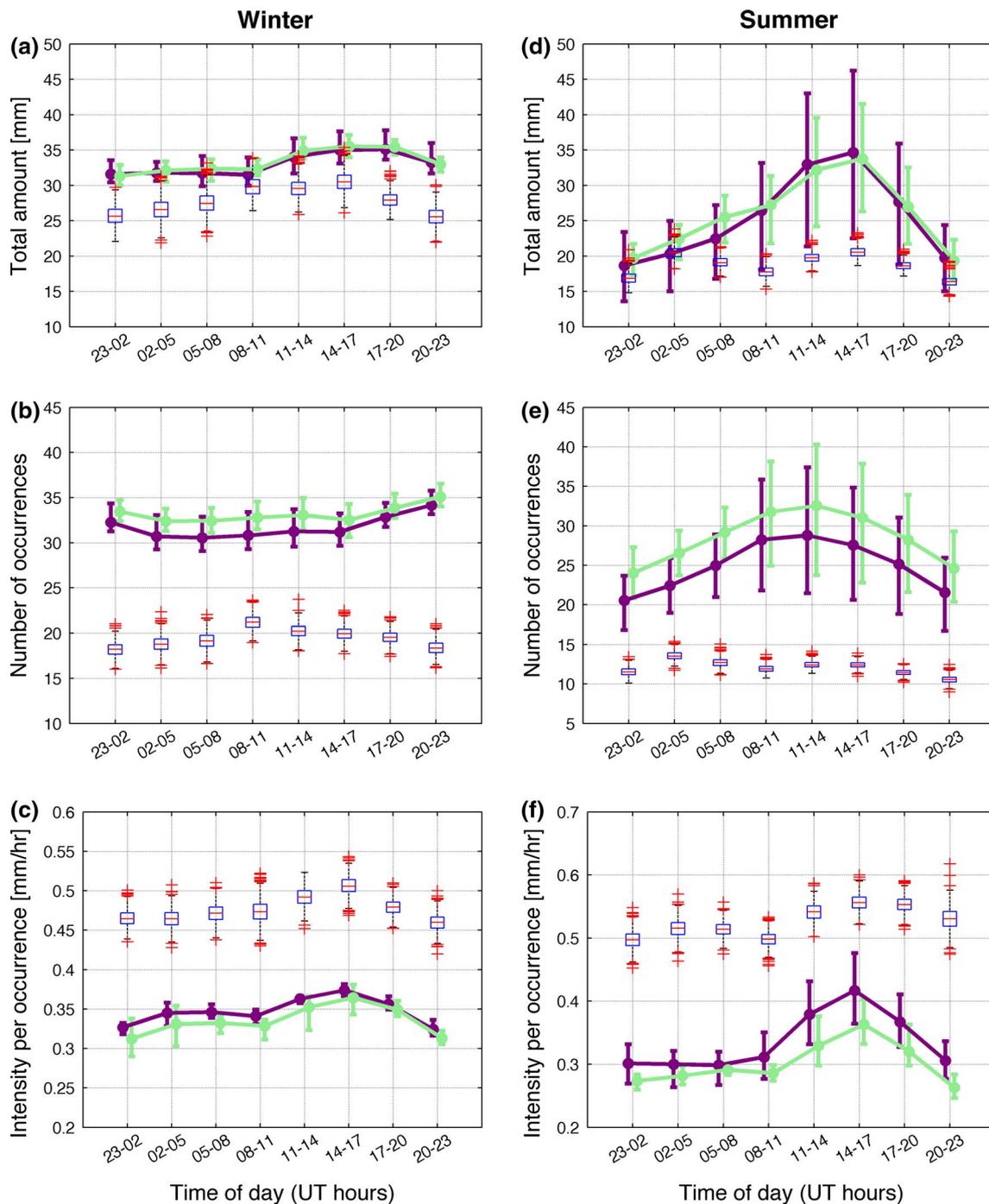
Fig. 3 a–c Observed (*boxplots*) and modelled (*lines*) diurnal cycle of precipitation: **a** total precipitation, **b** number of occurrences and **c** intensity per occurrence in each 3-h period in winter for the ensemble mean of the 6 simulations (see Table 1) that use the Noah LSM (*red*) and RUC LSM (*green*). *Error bars* on the simulations represent the maximum and minimum bounds of each ensemble mean. Points for Noah (RUC) LSM are offset by 30 min early (late) to improve the clarity of the plots. **d–f** As in **a–c** but for summer

4.3 Influence of radiation schemes

Similar to the microphysics schemes examined, the two longwave radiation schemes—rapid radiative transfer model (RRTM) and community atmosphere model (CAM)—do not influence WRF's ability to simulate the diurnal cycle of wintertime precipitation (Fig. 5a–c). In summer, the characteristics of the diurnal cycle are also unaffected by the longwave radiation schemes (Fig. 5d–f). Nonetheless, it is clear that simulations using CAM have a larger bias in the
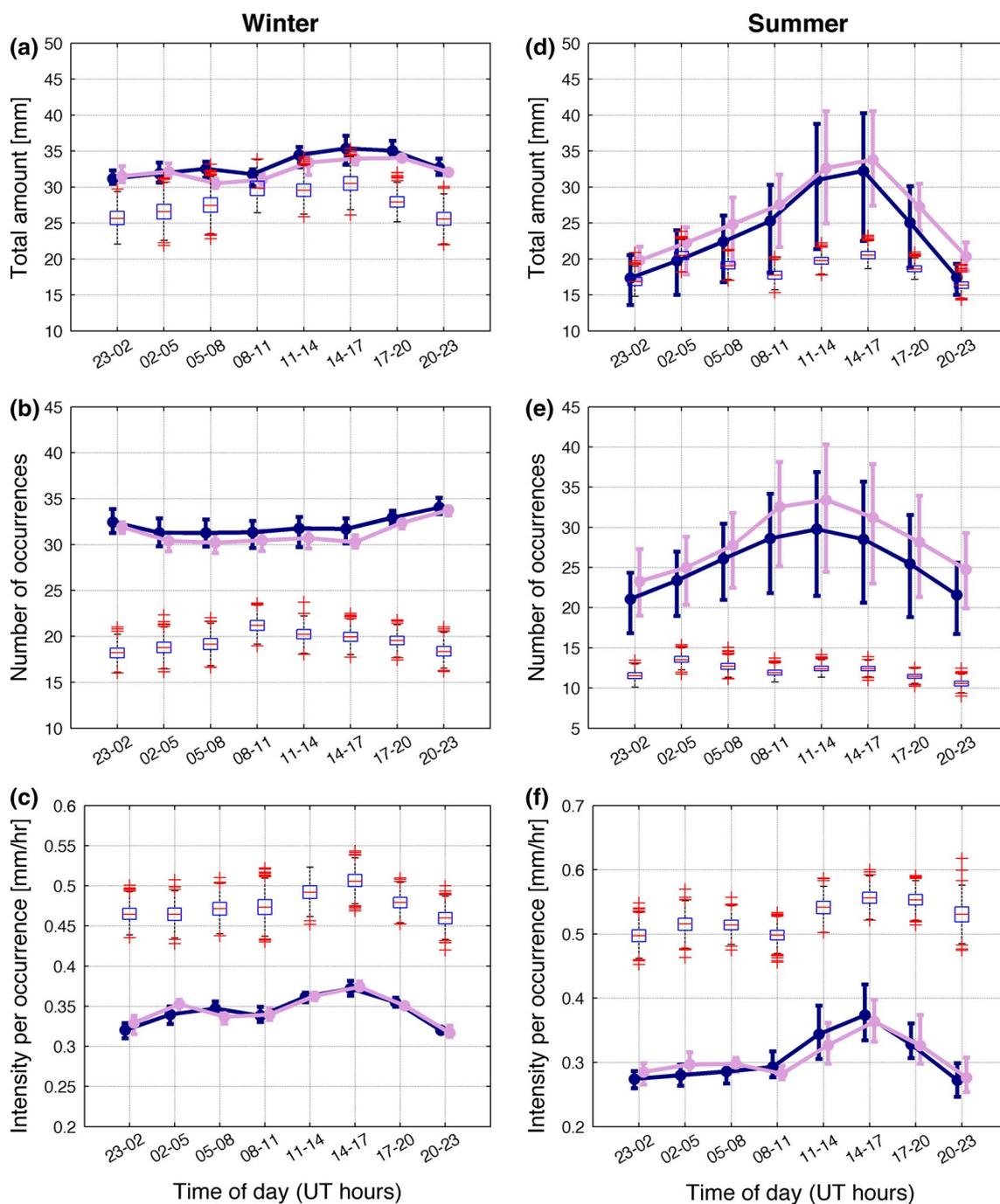
Fig. 4 a–c Observed (*boxplots*) and modelled (*lines*) diurnal cycle of precipitation: **a** total precipitation, **b** number of occurrences and **c** intensity per occurrence in each 3-h period in winter for the ensemble mean of the 4 simulations (see Table 1) that use the WSM3 microphysics (*grey*) and Morrison microphysics (*cyan*). *Error bars* on the simulations are the maximum and minimum bounds of each ensemble mean. Points for WSM3 (Morrison) scheme are offset by 30 min early (late) to improve the clarity of the plots. **d–f** As in **a–c** but for summer

number of occurrences compared with RRTM (Fig. 5e). However, this bias is offset in the total amounts of precipitation by the smaller intensity values of the simulations using RRTM (Fig. 5f). The large range of the six simulations for

each longwave radiation scheme in summer (indicated by the error bar in Fig. 5d and e) results from the difference between the LSMs (described in Sect. 4.1) in each group of six.

Fig. 5 **a–c** Observed (*boxplots*) and modelled (*lines*) diurnal cycle of precipitation: **a** total precipitation, **b** number of occurrences and **c** intensity per occurrence in each 3-h period in winter for the ensemble mean of the 6 simulations (see Table 1) that use the RRTM longwave radiation scheme (*purple*) and CAM longwave radiation scheme (*green*). *Error bars* on the simulations are the maximum and minimum bounds of each ensemble mean. Points for RRTM (CAM) scheme are offset by 30 min early (late) to improve the clarity of the plots. **d–f** As in **a–c** but for summer

4.4 Influence of planetary boundary layer schemes

Figure 6a–c show that the two PBL schemes employed in this study—Yonsei University (YSU) and the Mellor–Yamada Nakanishi and Niino level 3.0 (MYNN3)—do

not influence WRF's ability to simulate the diurnal cycle of winter precipitation. Furthermore, the diurnal cycle of summertime precipitation amounts and intensity are also unaffected by the PBL schemes. Only the diurnal cycle of occurrences is marginally influenced by the
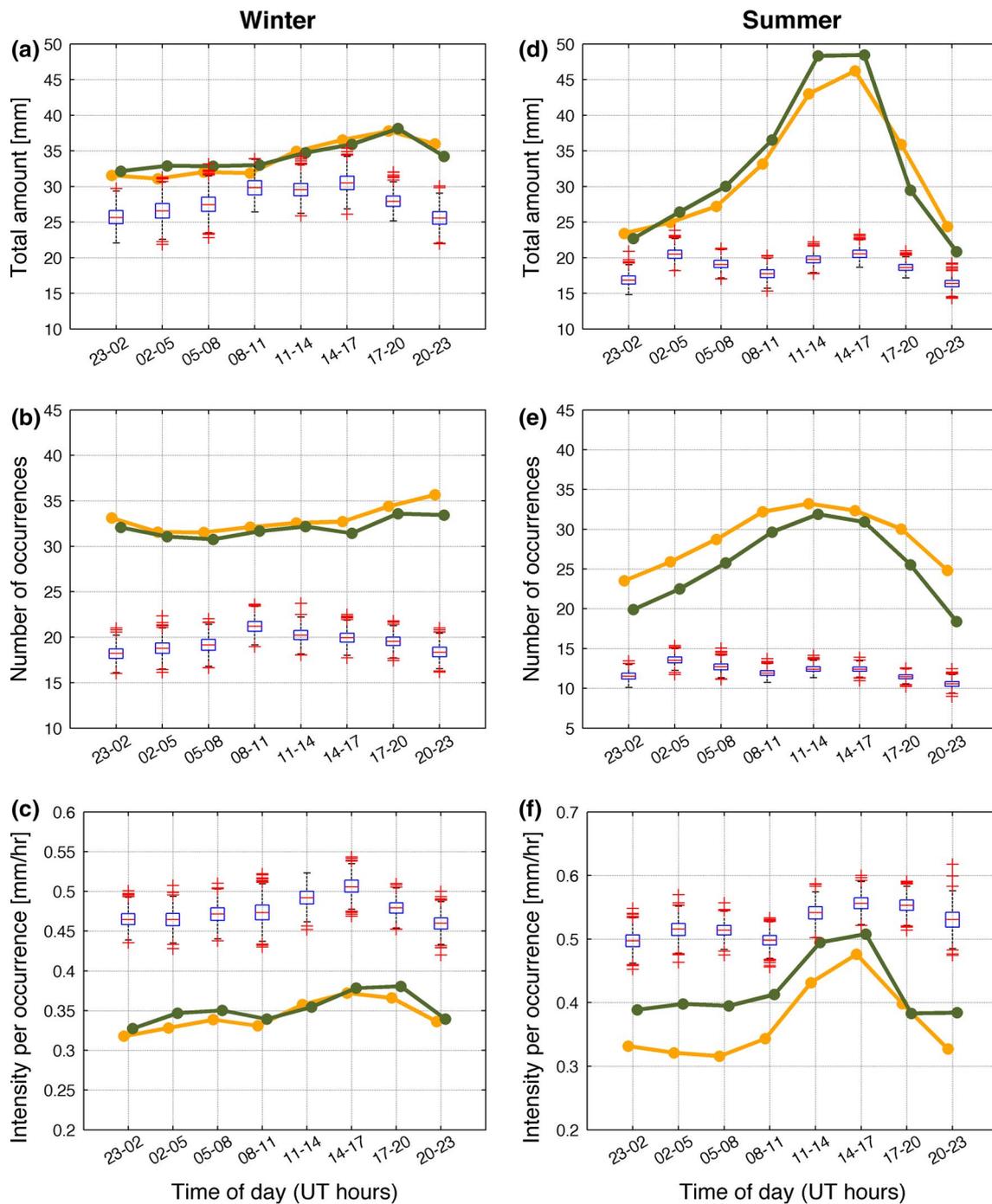
Fig. 6 a–c Observed (*boxplots*) and modelled (*lines*) diurnal cycle of precipitation: **a** total precipitation, **b** number of occurrences and **c** intensity per occurrence in each 3-h period in winter for the ensemble mean of the 6 simulations (see Table 1) that use the YSU PBL scheme

(navy) and MYNN3 PBL scheme (plum). *Error bars* on the simulations represent the maximum and minimum bounds of each ensemble mean. Points for YSU (MYNN3) scheme are offset by 30 min early (late) to improve the clarity of the plots. **d–f** As in **a–c** but for summer

PBL schemes. Once again, the large range of the four simulations for each PBL scheme (indicated by the error bar in Fig. 6d, e) in summer results from the difference between the LSMs (described in Sect. 4.1) in each group of four.

4.5 Influence of cumulus schemes

It can be seen in Fig. 7a–c that neither cumulus scheme has a significant impact on the simulated diurnal cycle in winter. Figure 7d–f show that in summer, the Betts–Miller–Janjic

Fig. 7 a–c Observed (*boxplots*) and modelled (*lines*) diurnal cycle of precipitation: **a** total precipitation, **b** number of occurrences and **c** intensity per occurrence in each 3-h period in winter for the simulation (see Table 1) using the Kain–Fritsch cumulus scheme (*yellow*) and Betts–Miller–Janjic cumulus scheme (*dark olive green*). Points for Kain–Fritsch (K–F) scheme are offset by 30 min early (late) to improve the clarity of the plots. **d–f** As in **a–c** but for summer

scheme produces marginally more precipitation than the Kain–Fritsch scheme. This results from producing slightly fewer occurrences and a higher intensity per occurrence than the Kain–Fritsch scheme. There is a small difference in the amplitude of the two simulated diurnal cycles of intensity but the timing of the peak is the same for both simulations. The simulated diurnal cycles of amount and occurrence in summer are also largely unaffected by the different cumulus schemes.

4.6 Influence of LSMs on convective precipitation, relative humidity and temperature

As shown in the previous sections, WRF's ability to simulate the summertime diurnal cycle is affected more by LSMs than either microphysics, PBL, cumulus or longwave radiation. The role of LSMs is to redistribute the incoming solar radiation flux between reflected solar radiation, surface longwave emission, latent and sensible heat fluxes, based on the principles of water balance and energy balance. The two LSMs examined here include a soil temperature scheme and moisture in four (Noah) or six (RUC) layers, frozen soil physics and either fractional snow cover (Noah) or multi-layer (RUC) snow. Soil levels in Noah are 10, 30, 60 and 100 cm, whereas those in RUC are 0, 5, 20, 40, 160 and 300 cm. Soil temperature and moisture in Noah are computed by a prognostic equation which includes the effects of snow cover and permafrost. RUC solves the thermal diffusion equation and Richards moisture equation at six layers to obtain soil temperature and moisture. The soil texture and vegetation types are the same for both LSMs with the WRF preprocessing package using 16 soil categories and the 24-category USGS land-cover dataset. Greater detail on the differences between the two LSMs are included in Zeng et al. (2012).

In this section we investigate the influence of the LSM on convective and non-convective precipitation, relative humidity at 2 m, surface temperature at 2 m and atmospheric profiles. Figure 8a–f show non-convective (left panels) and convective (right panels) precipitation in summer for total amounts, number of occurrences and intensity per occurrence. Both non-convective and convective precipitation are clearly influenced by the LSMs. The Noah LSM produces significantly greater amounts of precipitation and more occurrences than the RUC LSM. This is most pronounced near the peak of the cycle in the convective precipitation. Both types produce too much precipitation but convective precipitation clearly produces more near the afternoon peak. This suggests that convective processes are primarily responsible for the large discrepancy between the simulations and observations. Night time precipitation is dominated by the non-convective component with the total amounts and occurrences of non-convective precipitation showing an early morning peak. Conversely, daytime precipitation is dominated by convective precipitation which peaks in the late afternoon. This afternoon convective peak is much larger than the non-convective morning peak and this results in a single afternoon peak when both types are combined together and hence the dominant diurnal harmonic noted in Sect. 3. Figure 8c and f show that both convective and non-convective precipitation have a late afternoon peak in the intensity per occurrence.

Table 3 highlights a fundamental problem with both LSMs in summer; they are dominated by the 24-h component (~80 % explained variance) whereas the 12-h component is far more prevalent in the observations (~60 % explained variance). The main reason for a transition from a dominant 24-h component in winter to 12-h component in summer is the presence of an early morning peak in precipitation which is not observed in winter. An early morning precipitation peak has been reported by several authors, e.g., Kiely et al. (1998), Svensson and Jakob (2002), Twardosz (2007) and Walther et al. (2013). Considering only the non-convective precipitation from the WRF simulations improves the agreement with the observations (the two right-hand columns in Table 3) by reducing the large bias, but it does not address the imbalance in the ratio of the 24–12-h component.

Figure 9a, b show the modelled and observed diurnal cycle of relative humidity (RH %) at 2 m in both winter and summer respectively, while Fig. 10a, b show the corresponding temperature data at 2 m (T2). The observed relative humidity has a maximum in the early morning and a minimum in the early afternoon, while temperature observations at 2 m show a minimum at dawn and a maximum in the afternoon in agreement with Rohan (1987). Brockhaus et al. (2008) have pointed out that the diurnal cycle of specific humidity can be interpreted as an evaporation driven peak with a superimposed dip at the time of maximum PBL growth and associated entrainment of dry air from above. WRF simulations accurately capture the amplitude of both the RH % and T2 cycles and the timings of their peaks and trough as shown in Figs. 9 and 10. Simulations that use the RUC LSM yield RH % values that are very close to the observations in summer whereas Noah values are ~8 % too high at the dip. The corresponding T2 values for Noah are approximately 2 °C too low at the dip whereas RUC values again agree quite well with the observations as shown in Fig. 10b. The combination of excess humidity and lower temperatures are a likely cause of the large precipitation bias when using the Noah LSM in summer (Fig. 3d) compared with RUC values. Similar results were reported by Brockhaus et al. (2008) who compared diurnal cycles from the community land model (CLM) regional climate model with hourly data at several stations in Switzerland. They noted an underestimation of the diurnal temperature range and a cold bias of 1–3 K, which resulted in a boundary layer that is too shallow. A cold bias in diurnal temperature was observed in GCM-driven simulations of CLM for most of western Europe by Jacob et al. (2007). However, the British Isles and Eastern Europe were found to be exceptions in that instance.

In our results for winter the situation is reversed with Noah values of RH % and T2 closer to the observations than RUC. However, differences between simulations using
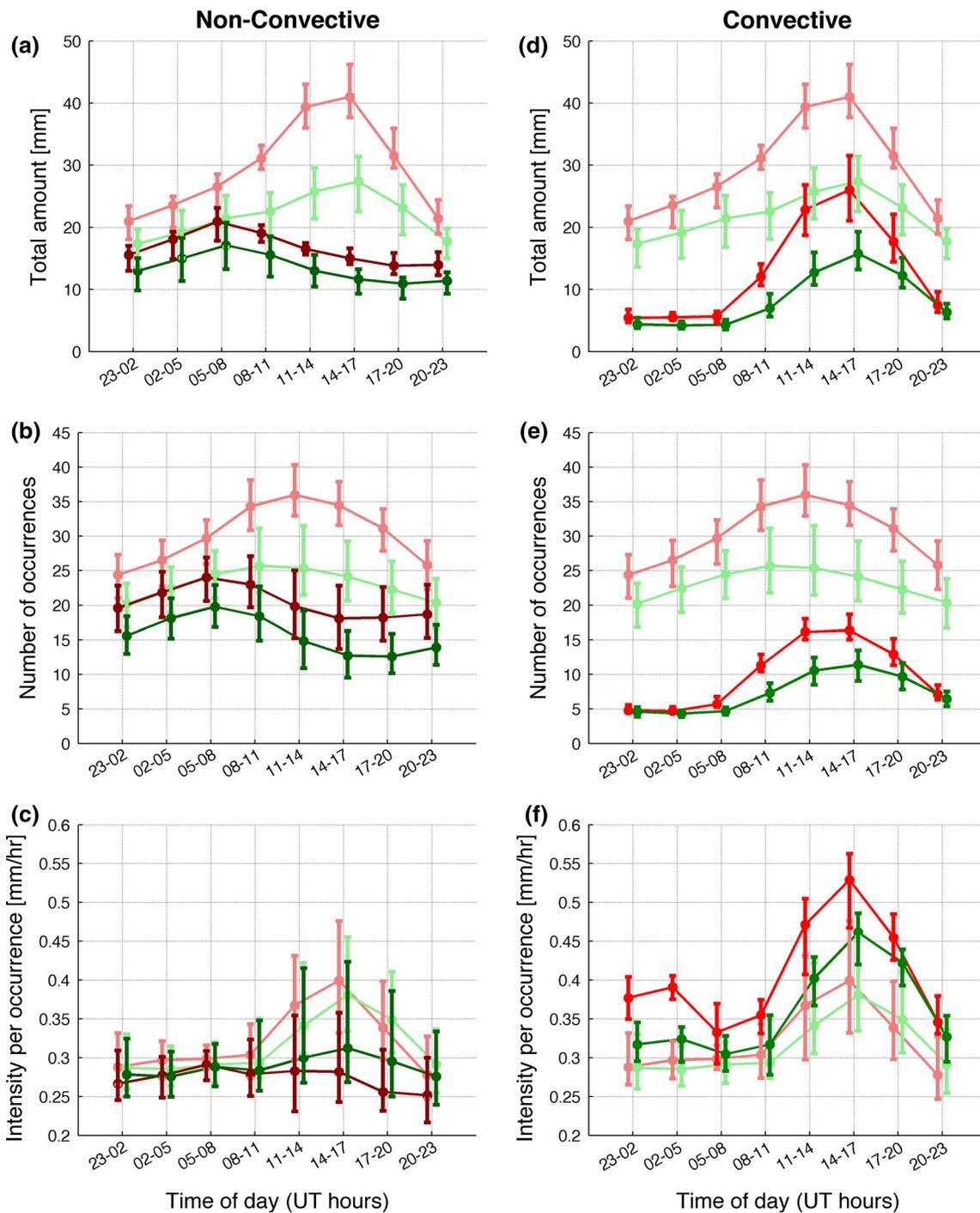
Fig. 8 **a–c** Diurnal cycle of non-convective and total precipitation modelled by WRF: **a** total precipitation, **b** number of occurrences and **c** intensity per occurrence in each 3-h period in summer for the ensemble mean of the simulations that use the Noah LSM (*dark red* for non-convective precipitation and faded red for total precipitation) and RUC LSM (*dark green* for non-convective precipitation and faded green for total precipitation). *Error bars* on the simulations represent the maximum and minimum bounds of each ensemble mean. Points for Noah (RUC) LSM are offset by 30 min early (late) to improve the clarity of the plots. **d–f** As in **a–c** but for convective precipitation

RUC and Noah LSM are negligible in winter with both yielding precipitation amounts that are approximately 40 % too high throughout the diurnal cycle. Winter precipitation

in the British Isles is dominated by orographic and frontal precipitation with relatively small contributions from convective precipitation (de Leeuw et al. 2014). Since winter

Table 3 Results of harmonic analysis of observed and WRF simulated total, convective and non-convective precipitation for summer only with Noah and RUC LSMs

	Observed	WRF Total precip.		WRF convective precip.		WRF Non-convective	
		Noah LSM	RUC LSM	Noah LSM	RUC LSM	Noah LSM	RUC LSM
Summer precipitation							
Diurnal average (mm)	18.7 (1.6)	29.4 (8.2)	21.8 (3.6)	13.6 (8.4)	8.2 (4.4)	16.0 (2.2)	13.4 (2.4)
24-h amplitude (mm)	1.0 (0.3)	9.8 (0.2)	4.5 (0.2)	10.4 (0.2)	5.6 (0.1)	2.9 (0.2)	3.1 (0.1)
24-h phase (h)	11.2 (1.1)	−10.5 (0.04)	−10.6 (0.1)	−9.3 (0.01)	−8.5 (0.01)	8.3 (0.3)	7.0 (0.1)
12-h amplitude (mm)	1.8 (0.3)	3.1 (0.2)	1.6 (0.2)	3.8 (0.2)	1.6 (0.1)	0.6 (0.2)	0.5 (0.1)
12-h phase (h)	3.8 (0.4)	3.1 (0.2)	3.9 (0.2)	2.9 (0.1)	3.5 (0.1)	−3.6 (0.3)	−5.3 (0.2)
Explained variance							
Diurnal (24-h)	22 %	80 %	77 %	77 %	81 %	83 %	85 %
Semidiurnal (12-h)	61 %	8 %	10 %	10 %	7 %	4 %	2 %

The figures in parentheses are the $1 - \sigma$ uncertainties on the quoted values estimated from the least-squares fit. The percentage values in the rows labeled diurnal (and semidiurnal) amplitude are the contribution of that component to the variance
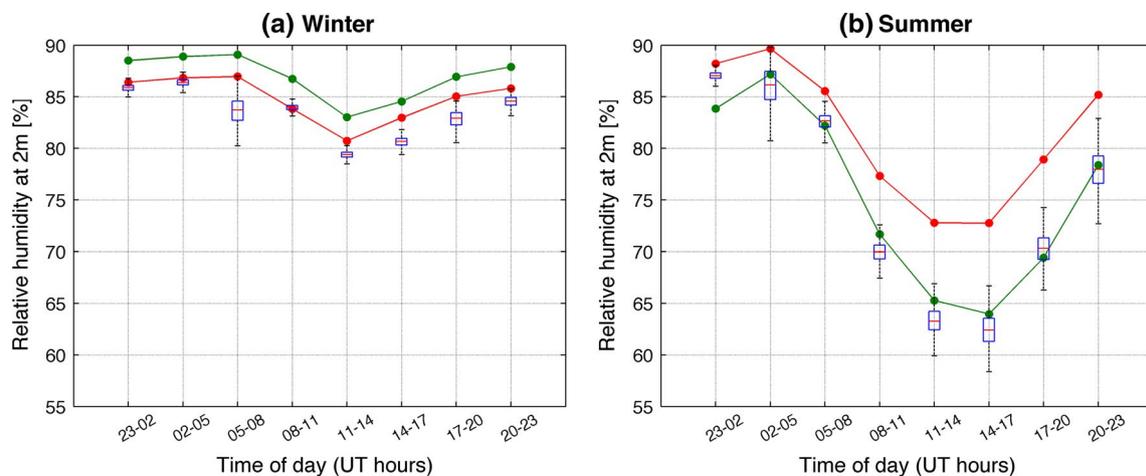

Fig. 9 a Relative humidity in winter (observed—*boxplots*) and the ensemble mean of the WRF simulations (*lines*) with the Noah LSM (*red line*) and RUC LSM (*green line*). **b** As in **a** except for summer
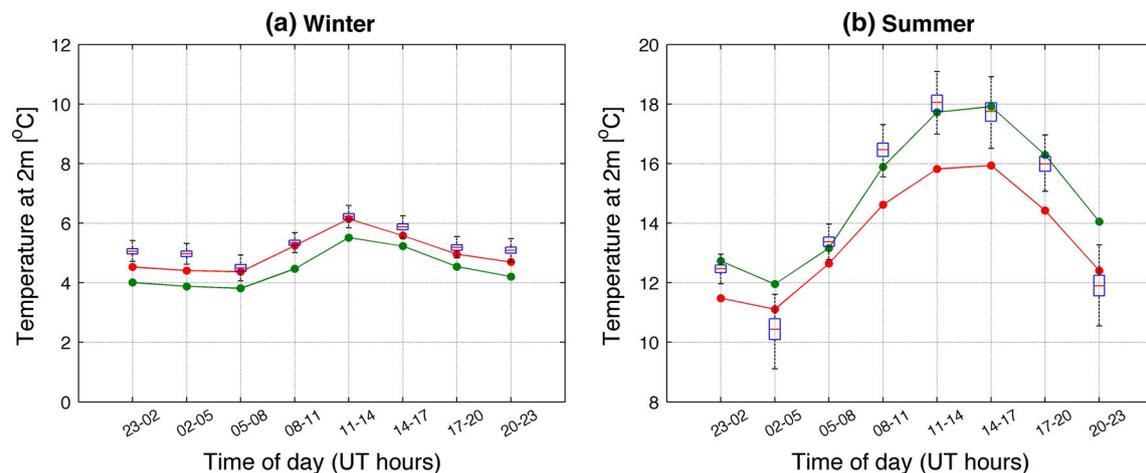
Fig. 10 a Surface air temperature in winter (observed—*boxplots*) and the ensemble mean of the WRF simulations (*lines*) with the Noah LSM (*red line*) and RUC LSM (*green line*). **b** As in **a** except for summer

Fig. 11 **a–f** Skew-T/log-P plots of atmospheric profiles from a simulation using NOAH (*red*; W3_Ys_No_Rr) a corresponding simulation using RUC (*green*; W3_Ys_Ru_Rr) and observed radiosondes (*blue*) in the boundary layer at Camborne (*row 1*), Hillsborough (*row 2*) and Stornoway (*row 3*) at midnight and midday for summer over the period 1990–1995
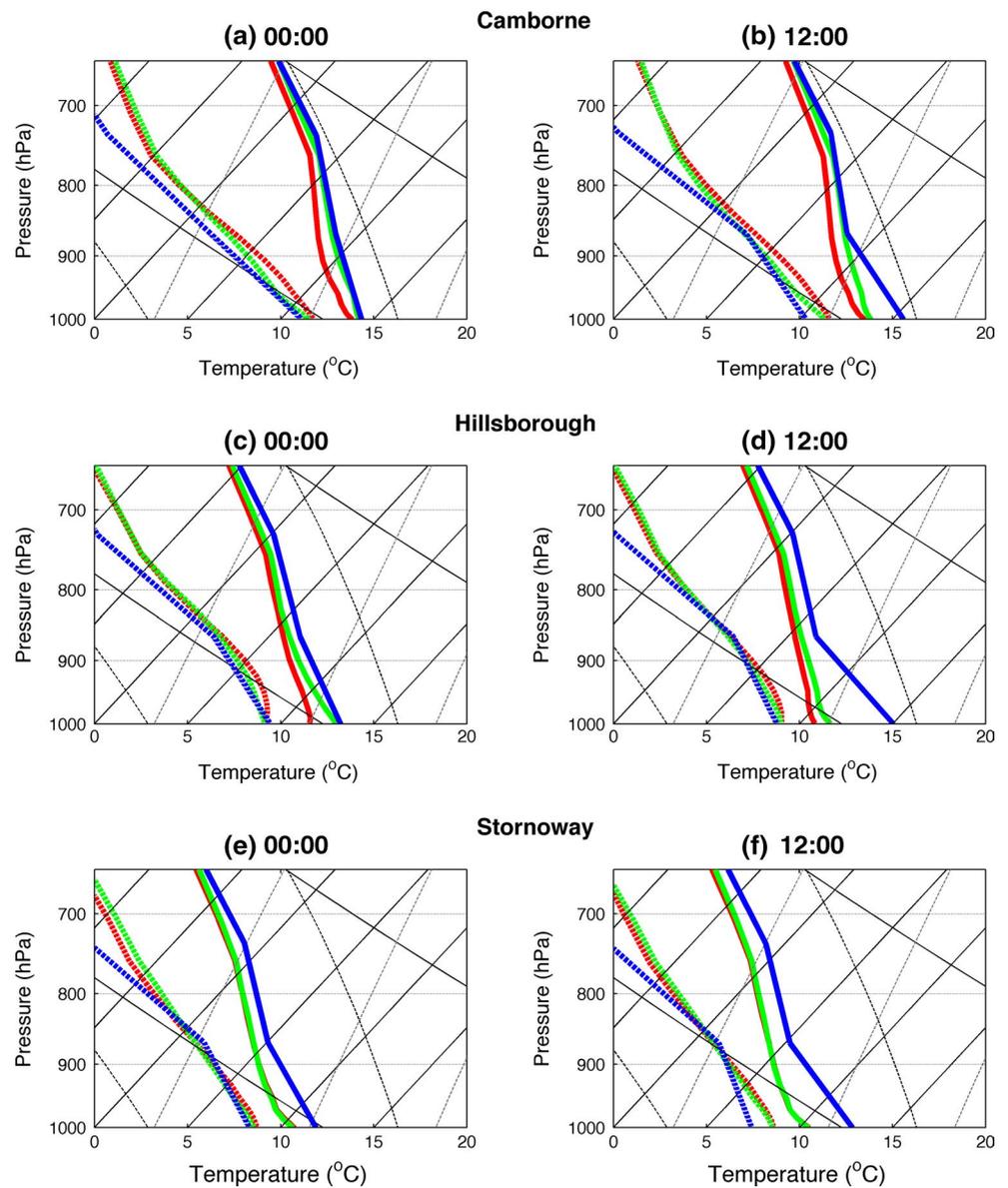
precipitation is predominantly a result of large-scale atmospheric processes, the modelled diurnal cycle is mostly unaffected by parameterizations.

Previous research (Brockhaus et al. 2008) on the possible links between biases in atmospheric profiles and triggering of convective precipitation showed that lower atmospheric temperatures would reduce water holding capacity and increase the likelihood of precipitation. Figure 11 shows skew-T/logP plots at midnight and midday for observed and modelled data at three stations during summer in our domain. The modelled data in these plots show two WRF simulations that are representative of those simulations which use NOAH (W3_Ys_No_Rr) and those which use RUC (W3_Ys_Ru_Rr). In general, modelled atmospheric temperatures are colder than observations, and modelled

dewpoint temperatures are higher than the corresponding observations at the surface and at higher altitudes (results for Stornoway shown in row 3 of Fig. 11 are atypical in this respect). This is consistent with the higher levels of precipitation predicted by the simulations compared with observed values. Near the surface, atmospheric profiles using Noah tend to have lower temperatures and higher dewpoint temperatures than those that using RUC, which is again consistent with the results shown in Figs. 9b and 10b. Our results are also consistent with observations of Jin et al. (2010) in which land surface processes were found to strongly affect temperature simulations, which impacted precipitation. Differences between the two sets of simulated profiles are reduced at higher levels. Examination of skew-T plots for all stations up to a pressure level of 100 hPa (not shown)

indicates good agreement between simulated and observed environmental temperatures. However, modelled dew-point temperatures are 2–5 °C higher than observed values which could explain the increased frequency of modelled precipitation.

5 Summary

We have simulated the diurnal cycle of precipitation in both summer and winter over the British Isles using the WRF model for thirteen different parameterization combinations—two LSMs, two microphysics schemes, two radiation schemes, two cumulus and two PBLs. In all cases, WRF significantly overestimates precipitation, in some instances by more than 100 %. There are too many occurrences of precipitation and the intensity per occurrence is too low in every simulation. Possible explanations for this include grid spacing, an overly sensitive trigger mechanism in the convective scheme and a wet bias in the driving data. A wet bias in the driving data is an unlikely explanation as analysis of the diurnal cycle in ERA-Interim does not show a wet bias. Increasing the model horizontal resolution has been shown to reduce a wet bias (Kendon et al. 2012; Walther et al. 2013; Dirmeyer et al. 2012), but it is only when it reaches 'convection resolving' values that the improvement is clearly observed. Since winter precipitation in the British Isles is predominantly a result of large-scale atmospheric processes—a point supported by our parameterization results—model resolution alone is unlikely to be the origin of the wet winter bias in WRF. This is supported by the work of Chin et al. (2010) who examined the wet winter bias in WRF over California. Their investigation of the influence of grid resolution (12 and 2 km) on the bias showed that low resolution runs tended to underpredict precipitation in coastal regions and overpredict it elsewhere in California while the high resolution simulations increased model precipitation everywhere.

Summer precipitation in the British Isles receives a greater contribution from convective processes compared with winter and is subject to more small scale effects. As a result, parameterizations have a greater influence in this season.

Of the parameterizations examined here—land surface schemes, microphysics, longwave radiation, cumulus, and PBL—only the land surface schemes had a significant influence on the diurnal cycle of precipitation, and only in the summer season. Simulations involving the Noah LSM produced total precipitation amounts that were on average up to 7 % (40 %) further from the observations than RUC in winter (summer).

In an effort to understand the impact of LSMs in the warm season, we examined the diurnal cycle of convective and non-convective precipitation, temperature and relative humidity. We found that Noah produced convective precipitation more frequently, had colder surface temperatures and higher humidity than RUC in summer. Skew-T profiles showed very little difference between simulations that used the Noah LSM and RUC LSM at higher levels. These results suggest that the WRF simulations with the Noah LSM could be overestimating evapotranspiration at the expense of sensible heat (Brockhaus et al. 2008). In conclusion, this study has shown that accurately reproducing the diurnal cycle of precipitation remains a challenge with a clear need for more studies on the detailed regional characteristics and the physical mechanisms that underlie the cycle.

References

Alexander LV, Jones PD (2000) Updated precipitation series for the U.K. and discussion of recent extremes. Atmos Res Lett 1(2):142–150

Argüeso D, Hidalgo-Muñoz JM, Gámiz-Fortis AR, Esteban-Parra MJ, Dudhia J, Castro-Díez Y (2011) Evaluation of WRF parameterizations for climate studies over Southern Spain using a multistep regionalization. J Clim 24:5633–5651. doi:10.1175/JCLI-D-11-00073.1

Betts AK (1986) A new convective adjustment scheme. Part I. Observational and theoretic basis. Q J R Meteorol Soc 112:677–691

Betts AK, Miller MJ (1986) A new convective adjustment scheme. Part II: single column tests using GATE wave, BOMEX, ATEX and arctic air-mass data sets. Q J R Meteorol Soc 112:693–709

Brockhaus P, Lüthi D, Schär C (2008) Aspects of the diurnal cycle in a regional climate model. Meteorol Z 17(4):433–443

Bukovsy MS, Karoly DJ (2009) Precipitation simulations using WRF as a nested regional climate model. J Appl Meteorol Clim 48:2152–2159. doi:10.1175/2009JAMC2186.1

Bukovsy MS, Karoly DJ (2011) A regional modeling study of climate change impacts on warm-season precipitation in the central united states. J Clim 24:1985–2002

Carbone RE, Tuttle JD, Ahijevych DA, Trier SB (2002) Inferences of predictability associated with warm season precipitation episodes. J Atmos Sci 59:2033–2056

Chin H-NS, Caldwell PM, Bader DC (2010) Preliminary study of California wintertime model wet bias. Mon Weather Rev 138:3556–3571

Christensen JH, Christensen OB (2007) A summary of the PRUDENCE model projections of changes in European climate by the end of this century. Clim Change 81:7–30. doi:10.1007/s10584-006-9210-7

Clarke AJ, Gallus WA, Chen T-C (2007) Comparison of the diurnal precipitation cycle in convection-resolving and non-convection-resolving mesoscale models. Mon Weather Rev 135:3456–3473

Collier JC, Bowman KP (2004) Diurnal cycle of tropical precipitation in a general circulation model. J Geophys Res 109:D17105. doi:10.1029/2004JD004818

Collins WD, Rasch PJ, Boville BA, Hack JJ, McCaa JR, Williamson DL, Kiehl JT, Briegleb B, Bitz C, Lin S-J, Zhang M., Dai Y (2004) Description of the NCAR community atmosphere model (CAM 3.0). NCAR Technical Note, TN-464+STR, pp 102–143

Dai A (2001a) Global precipitation and thunderstorm frequencies. Part I: seasonal and interannual variations. J Clim 14:1092–1111

Dai A (2001b) Global precipitation and thunderstorm frequencies. Part II: diurnal variations. J Clim 14:1112–1128

Dai A, Deser C (1999) Diurnal and semidiurnal variations in global surface wind and divergence fields. J Geophys Res 104:31109–31125

Dai A, Trenberth KE (2004) The diurnal cycle and its depiction in the community climate system model. J Clim 17:930–951

Dai A, Wang J (1999) Diurnal and semidiurnal tides in global surface pressure fields. J Atmos Sci 56:3874–3891

Dai A, Giorgi F, Trenberth KE (1999a) Observed and model-simulated diurnal cycles of precipitation over the contiguous United States. J Geophys Res 104(D6):6377–6402

Dai A, Trenberth KE, Karl TR (1999b) Effects of clouds, soil moisture, precipitation and water vapor on diurnal temperature range. J Clim 12:2451–2473

Dai A, Lin X, Hsu K-L (2007) The frequency, intensity, and diurnal cycle of precipitation in surface and satellite observations over low- and mid-latitudes. Clim Dyn 29:727–744. doi:10.1007/s00382-007-0260-y

de Leeuw JJ, Methven J, Blackburn M (2014) Evaluation of ERA-Interim reanalysis precipitation products using England and Wales observations. Q J R Meteorol Soc. doi:10.1002/qj.2395

Dee DP, Uppala SM, Simmons AJ, Berrisford P, Poli P, Kobayashi S, Andrae U, Balmaseda MA, Balsamo G, Bauer P, Bechtold P, Beljaars ACM, van de Berg L, Bidlot J, Bormann N, Delsol C, Dragani R, Fuentes M, Geer AJ, Haimberger L, Healy SB, Hersbach H, Hólm EV, Isaksen L, Kållberg P, Köhler M, Matricardi M, McNally AP, Monge-Sanz BM, Morcrette J-J, Park B-K, Peubey C, de Rosnay P, Tavolato C, Thépaut J-N, Vitart F (2011) The ERA-Interim reanalysis: configuration and performance of the data assimilation system. Q J R Meteorol Soc 137:553–597. doi:10.1002/qj.828

Dirmeyer PA, Cash B, Kinter JL III, Jung T, Marx L, Satoh M, Stan C, Tomita H, Towers P, Wedi N, Achuthavarier D, Adams JM, Altshuler EL, Huang B, Jin EK, Manganello J (2012) Simulating the diurnal cycle of rainfall in global climate models: resolution versus parameterization. Clim Dyn 39:399–418. doi:10.1007/s00382-011-1127-9

Diro GT, Raischer SA, Giorgi F, Tompkins AM (2012) Sensitivity of seasonal climate and diurnal precipitation over Central America to land and sea surface schemes in RegCM4. Clim Res 52:31–48. doi:10.3354/cr01049

Ek M, Mahrt L (1991) OSU 1-D PBL model user's guide. Version 1.04. Department of Atmospheric Sciences, Oregon State University, Corvallis

Evans J, Westra S (2012) Investigating the mechanisms of diurnal rainfall variability using a regional climate model. J Clim 25:7232–7247. doi:10.1175/JCLI-D-11-00616.1

Gianotti RL, Zhang D, Eltahir EAB (2012) Assessment of the regional climate model version 3 over the maritime continent using different cumulus parameterization and land surface schemes. J Clim 25:638–656

Hong S-Y, Dudhia J, Chen S-H (2004) A revised approach to ice microphysical processes for the bulk parameterization of clouds and precipitation. Mon Weather Rev 132:103–120

Hong S-Y, Noh Y, Dudhia J (2006) A new vertical diffusion package with an explicit treatment of entrainment processes. Mon Weather Rev 134:2318–2341

Jacob D, Barring L, Christensen OB, Christensen JH, de Castro M, Deque M, Giorgi F, Hagemann S, Hirschi M, Jones R, Kjellstom E, Lenderink G, Rockel B, Sanchez E, Schar C, Seneviratne SI, Somot S, van Ulden A, van den Hurk B (2007) An inter-comparison of regional climate models for Europe: model performance in present-day climate. Clim Change 81:31–52. doi:10.1007/s10584-006-9213-4

Jaeger EB, Anders I, Lüthi D, Rockel B, Schär C, Seneviratne SI (2008) Analysis of ERA40-driven CLM simulations for Europe. Meteorol Z 17(4):349–367

Janjic ZI (1994) The step-mountain eta coordinate model: further developments of the convection, viscous sublayer, and turbulence closure schemes. Mon Weather Rev 122:927–945

Jeong J-H, Walther A, Nikulin G, Chen D, Jones C (2011) Diurnal cycle of precipitation amount and frequency in Sweden: observation versus model simulation. Tellus A 63:664–674. doi:10.1111/j.1600-0870.2011.00517.x

Jin J, Miller NL, Schlegel N (2010) Sensitivity Study of four land surface schemes in the WRF model. Adv Meteorol. Article ID 167436. doi:10.1155/2010/167436

Jones MR, Blenkinsop S, Fowler HJ, Kilsby CG (2014) Objective classification of extreme rainfall regions for the UK and updated estimates of trends in regional extreme rainfall. Int J Climatol 34:751–765

Kain JS (2004) The Kain–Fritsch convective parameterization: an update. J Appl Meteorol 43:170–181

Kain JS, Fritsch JM (1990) A one-dimensional entraining/detraining plume model and its application in convective parameterization. J Atmos Sci 47:2784–2802

Katragkou E, García-Díez M, Vautard R, Sobolowski S, Zanis P, Alexandri G, Cardoso RM, Colette A, Fernandez J, Gobiet A, Goergen K, Karacostas T, Knist S, Mayer S, Soares PMM, Pytharoulis I, Tegoulias I, Tsikerdekis A, Jacob D (2015) Regional climate hindcast simulations within EURO-CORDEX: evaluation of a WRF multi-physics ensemble. Geosci Model Dev 8:603–618. doi:10.5194/gmd-8-603-2015

Kendon EJ, Roberts NM, Senior CA, Roberts MJ (2012) Realism of rainfall in a very high-resolution regional climate model. J Clim 25(17):5791–5806. doi:10.1175/JCLI-D-11-00562.1

Kiely G, Albertson JD, Parlang MB (1998) Recent trends in diurnal variation of precipitation at Valentia on the west coast of Ireland. J Hydrol 207:270–279

Kikuchi K, Wang B (2008) Diurnal precipitation regimes in the global tropics. J Clim 21:2680–2696. doi:10.1175/2007JCLI2051.1

Lee M-I, Schubert SD, Suarez MJ, Held IM, Kumar A, Bell TL, Schemm JKE, Lau NC, Ploshay JJ, Kim HK, Yoo SH (2007) Sensitivity to horizontal resolution in the AGCM simulations of warm season diurnal cycle of precipitation over the United States and Mexico. J Clim 20:1862–1881

Lee M-I, Schubert SD, Suarez MJ, Schemm J-KE, Pan H-L, Han J, Yoo S-H (2008) Role of convection triggers in the simulation of the diurnal cycle of precipitation over the United States Great Plains in a general circulation model. J Geophys Res 113:D02111

Liang X-Z, Li L, Dai A, Kunkel KE (2004) Regional climate model simulation of summer precipitation diurnal cycle over the United States. Geophys Res Lett 31:L24208

Mapes B, Warner T, Xu M (2003) Diurnal patterns of rainfall in northwestern South America III. Diurnal gravity waves and nocturnal convection offshore. Mon Weather Rev 131:830–844

Mellor GL, Yamada T (1982) Development of a turbulence closure model for geophysical fluid problems. Rev Geophys Space Phys 20:851–875

Met Office (2006) Met Office high resolution radiosonde data from the UK, Gibralta, St Helena and the Falkland Islands. NCAS British Atmospheric Data Centre, 10 April 2015. http://catalogue.ceda.ac.uk/uuid/c1e2240c353f8edeb98087e90e6d832e

Met Office (2012) Met Office Integrated Data Archive System (MIDAS) Land and marine surface stations data (1853-current). NCAS British Atmospheric Data Centre, 18 December 2013, http://catalogue.ceda.ac.uk/uuid/220a65615218d5c9cc9e4785a3234bd0

Mlawer EJ, Taubman SJ, Brown PD, Iacono MJ, Clough SA (1997) Radiative transfer for inhomogeneous atmosphere: RRTM, a validated correlated-k model for the longwave. J Geophys Res 102:16663–16682

Mooney PA, Mulligan FJ, Fealy R (2013) Evaluation of the sensitivity of the Weather Research and Forecasting model to parameterization schemes for regional climates of Europe over the period 1990–1995. J Clim 26:1002–1017. doi:10.1175/JCLI-D-11-00676.1

Morrison H, Thompson G, Tatarskii V (2009) Impact of cloud microphysics on the development of trailing stratiform precipitation in a simulated squall line: comparison of one- and two-moment schemes. Mon Weather Rev 137:991–1007

Nakanishi M, Niino H (2004) An improved Mellor–Yamada level-3 model with condensation physics: its design and verification. Bound Layer Meteorol 112:1–31

Oki T, Musiake K (1994) Seasonal change of the diurnal cycle of precipitation over Japan and Malaysia. J Appl Meteorol 33:1899–1922

Peel MC, Finlayson BL, McMahon TA (2007) Updated world map of the Köppen–Geiger climate classification. Hydrol Earth Syst Sci 11:1633–1644. doi:10.5194/hess-11-1633-2007

Perez JC, Díaz JP, González A, Expósito J, Rivera-López F, Taima D (2014) Evaluation of WRF parameterizations for dynamical downscaling in the Canary Islands. J Clim 27(14):5611–5631. doi:10.1175/JCLI-D-13-00458.1

Rauscher SA, Coppola E, Piani C, Giorgi F (2010) Resolution effects on regional climate model simulations of seasonal precipitation over Europe. Clim Dyn 35:685–711. doi:10.1007/s00382-009-0607-7

Rohan PK (1987) The climate of Ireland, 2nd edn. Stationery Office, Dublin

Skamarock WC, Klemp JB, Dudhia J, Gill DO, Barker DM, Duda MG, Huang X-Y, Wang W, Powers JG (2008) A Description of the Advanced Research WRF Version 3. NCAR Technical Note, NCAR, Boulder, CO, USA

Smirnova TG, Brown JM, Benjamin SG (1997) Performance of different soil model configurations in simulating ground surface temperature and surface fluxes. Mon Weather Rev 125:1870–1884

Smirnova TG, Brown JM, Benjamin SG, Kim D (2000) Parameterization of cold-season processes in the MAPS land surface scheme. J Geophys Res 105:4077–4086

Svensson C, Jakob D (2002) Diurnal and seasonal characteristics of precipitation at an upland site in Scotland. Int J Climatol 22:587–598

Twardosz R (2007) Seasonal characteristics of diurnal precipitation variation in Kraków (South Poland). Int J Climatol 27:957–968

Wallace J (1975) Diurnal variations in precipitation and thunderstorm frequency over the conterminous United States. Mon Weather Rev 103:406–419

Walther A, Jeong J-H, Nikulin G, Jones C, Deliang C (2013) Evaluation of the warm season diurnal cycle of precipitation over Sweden simulated by the Rossby Centre regional climate model RCA3. Atmos Res 119:131–139. doi:10.1016/j.atmosres.2011.10.012

Yang G, Slingo J (2001) The diurnal cycle in the tropics. Mon Weather Rev 129:784–801

Yaqub A, Seibert P, Formayer H (2011) Diurnal precipitation cycle in Austria. Theor Appl Climatol 103:109–118. doi:10.1007/s00704-010-0281-z

Zeng X-M, Wu Z-H, Song S, Xiong S-Y, Zheng Y-Q, Zhou Z-G, Liu H-Q (2012) Effects of different land-surface schemes on the simulation of a heavy rainfall event by WRF. Chin J Geophys 55(4):394–408